Optimization of Secondary-Air Addition in a Continuous One-Dimensional Spray Combustor

Justin A. Sirignano,* Luis Rodriguez,† Athanasios Sideris,‡ and William A. Sirignano§
University of California, Irvine, Irvine, California 92697-3975

A framework is established for optimal control of continuous combustors using the sequential linear quadratic algorithm. An analysis is presented for liquid-fuel vaporization and burning in a continuous combustor with secondary-air addition at downstream locations. A steady one-dimensional flow is portrayed and a system of nonlinear ordinary differential equations is established. Three combustion models are presented with different rate-controlling processes: vaporization, vaporization-mixing, and vaporization-mixing-reaction. The models have a sufficient number of characteristic times and sufficient nonlinearity to provide a challenge to an optimization procedure. The proposed method yields an optimal distribution of secondary-air addition.

Nomenclature

A^*	=	cross-sectional area, .01 m^2
c_p	=	specific heat of air, 1.3×10^3 J/(kg · K)
c_{v_l}	=	specific heat of liquid, 2.21×10^3 J/(kg · K)
La*	=	latent heat of vaporization, 2.63×10^5 J/kg
L^*	=	length of combustion chamber, 4 m
La	=	nondimensional latent heat of vaporization
$\dot{m}_f^*$	=	mass flow rate of fuel, kg/s
$\dot{m}_0^*$	=	inlet air mass flow rate, kg/s
$\dot{m}_1^*$	=	total added air mass flow rate, kg/s
p	=	pressure, 15 atm
Q^*	=	heating value of decane, 44.24×10^6 J/kg
R	=	nondimensional radius of droplet
Re	=	droplet Reynolds number
R_{air}^*	=	gas constant for air, 287.03 J/(kg · K)
R_{decane}^*	=	gas constant for decane, 58.549 J/(kg · K)
T_a	=	initial gas temperature, 900 K
T_b	=	nondimensional boiling point of decane
T_g	=	nondimensional gas temperature
T_l	=	nondimensional liquid temperature
u_g	=	nondimensional gas velocity
u_l	=	nondimensional liquid velocity
Y_F	=	fuel mass fraction
Y_O	=	air mass fraction
ν	=	stoichiometric mass ratio of fuel to air, 0.0679
μ_0^*	=	dynamic viscosity of air, 5×10^{-5} kg/(m · s)
ρ_g	=	nondimensional gas density
ρ_l	=	nondimensional liquid density

*Undergraduate Summer Intern, Department of Mechanical and Aerospace Engineering; jasirign@princeton.edu.
†Graduate Student, Department of Mechanical and Aerospace Engineering; larodrig@uci.edu.
‡Professor, Department of Mechanical and Aerospace Engineering; asideris@uci.edu.
§Professor, Department of Mechanical and Aerospace Engineering; sirignan@uci.edu.

I. Introduction

THE goal is to develop an approach that can be used for optimal control of a continuous spray combustor. Three simple models of spray combustion are constructed to explore the development of this formal optimization analysis. The focus is on the optimal control and not on the advancement of descriptive physical models. More sophisticated analyses of turbulent spray combustion can be easily found in the literature. For an overview, see Sirignano [1]. Nevertheless, the models used here have many characteristic times implying a certain robustness. Although these models will not describe all details of the spray combustion, they might adequately identify how to control the major input parameters in an optimal manner. And so, in this first effort, we begin with the simplest combustion models that we find to be physically reasonable in its global features.

Liquid fuel is injected at the upstream end of the combustor together with some air. The ratio of fuel to air is chosen to allow ignition and a stable flame. Additional air is added at downstream locations to keep the gas temperature at or below allowable levels. The system of two-phase flow equations for spray combustion [1] is simplified. Steady state is assumed. Averaging over the transverse dimensions reduces the system to a 1-D behavior, producing a system of ordinary differential equations. Heat and mass diffusion in the streamwise direction are neglected. The fuel is considered to have only one component rather than being a blend. An average droplet size is used in the model so that the size distribution of a practical spray is not portrayed. The mass flow rate for air addition is represented as a continuous function of downstream position. The goal is to vaporize and burn fully the fuel in the combustor chamber over the length. And so, we want to drive both the droplet radius and the fuel mass fraction to zero at the end of the combustor. Although total air addition is specified, the distribution of air addition is a control variable. Other variables, such as the initial average droplet radius, can also be a control variable. It is also desired to make the length of the combustor as short as possible, still maintaining the constraints and goal of complete combustion.

We considered three models of varying complexity for the combustion processes. In order of increasing complexity, the first (vaporization) model approximated vaporization as the dominant process for combustion, with the mixing of fuel vapor and air, as well as the chemical reaction between fuel vapor and air, taken as instantaneous following vaporization; in the second (vaporization-mixing) model we allow a finite time for the turbulent mixing as well as for vaporization; and in the third (vaporization-mixing-reaction) model all three processes, including now the chemical-reaction, will take a finite time to complete.

We focus on the optimal control problem of choosing the best profile (i.e., function) for the mass flow rate for air addition over the length of the combustion chamber. The mass flow rate for air addition is taken as a continuous function of downstream position. The total air addition is specified, so that by profile we mean the distribution of air addition. The optimal profile is the one that vaporizes and burns the maximum amount of fuel over the length of the combustion chamber, subject to the physics of the combustion and certain imposed constraints. Then, we set a target of zero for both the droplet radius and the fuel mass fraction at the end of the combustor. Using the sequential linear quadratic (SLQ) algorithm [2], we determine the optimal profile for the mass flow rate of air addition for the vaporization, vaporization-mixing, and vaporization-mixing-reaction models.

Some interesting optimization analysis for intermittent combustors has been performed by Ge et al., using a method that mimics evolutionary processes [3]. We are unaware of any formal optimization work on continuous combustors before our work. We distinguish here work on optimization from modelling attempts concerned with active control of combustion processes.

In Sec. II, we describe the models used in our study; in addition, the relationship between certain parameters and the amount of fuel burned is investigated through a parameter survey which attempts an informal optimization. The SLQ algorithm is explained in more detail in Sec. III. Our formal optimization results are presented in Sec. IV and the conclusions are summarized in Sec. V. Some details can be found in Appendices A and B and Sirignano et al. [4].

II. Models

We next briefly describe the three combustion models used in our study. In the following, R, u, T, and Y represent droplet radius, velocity, temperature, and mass fraction with the subscripts g, l, F, and O pertaining to gas phase, liquid phase, fuel vapor, and air. Quantities with asterisks are dimensional; subscript 0 implies inlet conditions. See the nomenclature at the beginning of this paper defining variables used. For numerical purposes (to avoid a singularity condition in the differential equations as R approaches zero), we construct our state variables as $z_1 = R^3$, $z_2 = R^3 u_l$, $z_3 = R^3 T_l$, $z_4 = u_g$, $z_5 = T_g$, $z_6 = Y_F$, and $z_7 = Y_O$. The first five quantities have been converted to a nondimensional form, using the initial values for droplet radius, gas velocity, and gas temperature to normalize. We add a final state $z_8 = \dot{m}_a$, which is the nondimensional amount of secondary-air flow rate between the inlet and position x. Its purpose is to force the nondimensional rate of air input $d\dot{m}_a/dx$ to integrate to the prescribed amount of air added over the length, namely, $\dot{m}_1^*/\dot{m}_0^*$; this is accomplished by fixing the final value

$$z_8(1) = \int_0^1 \frac{d\dot{m}_a}{dx'}\, dx' = \frac{\dot{m}_1^*}{\dot{m}_0^*}$$

as a constraint later in the optimization. From these state variables we form the state vector which yields eight simultaneous ordinary differential equations for the vaporization-mixing-reaction model:

$$\dot{\mathbf{z}} = \frac{d}{dx}\begin{pmatrix} z_1 \\ z_2 \\ z_3 \\ z_4 \\ z_5 \\ z_6 \\ z_7 \\ z_8 \end{pmatrix} = \frac{d}{dx}\begin{pmatrix} R^3 \\ R^3 u_l \\ R^3 T_l \\ u_g \\ T_g \\ Y_F \\ Y_O \\ m_a \end{pmatrix}$$

$$= \begin{pmatrix} -\frac{\tilde{\mu}\dot{M}}{u_{l0}} \\ \frac{\tilde{\mu}}{u_{l0}}[D - \dot{M}z_2/z_1] \\ \frac{\tilde{\mu}\dot{M}}{u_{l0}}[\frac{c_p}{c_{v_l}}L_{\text{eff}} - \frac{R^*}{c_{v_l}}\text{La} - z_3/z_1] \\ \frac{d\dot{m}_a}{dx} - \dot{M}L_{\text{eff}} + \kappa Q z_6 \\ \frac{z_5}{z_4}(1 - z_5)\frac{d\dot{m}_a}{dx} - \frac{z_5}{z_4}\dot{M}(L_{\text{eff}} + z_5) + \kappa Q z_6 \\ \frac{z_5}{z_4}\dot{M}(1 - z_6) - \frac{z_5}{z_4}\frac{d\dot{m}_a}{dx}z_6 - \kappa z_6 \\ \frac{z_5}{z_4}\frac{d\dot{m}_a}{dx}(1 - z_7) - \frac{z_5}{z_4}\dot{M}z_7 - \kappa\frac{z_6}{\nu} \\ U^2 \end{pmatrix} \quad (1)$$

In (1), $\tilde{\mu} = u_{l0} \cdot \dot{m}_0^*/\dot{m}_f^*$ is a nondimensional constant and

$$\kappa = \frac{L^*}{\sqrt{A^*} + z_4 \tau_{\text{chem}}}$$

where for decane

$$\tau_{\text{chem}} = 0.560091 \times 10^{-8}\frac{\mu_0^*}{\rho_0^{*3/4}L^*}T_g^{.75}e^{\frac{15106.2}{T_0^*}\frac{1}{T_g}}\frac{Y_F^{.75}}{Y_O^{1.50}}$$

with $\rho_0^* = (1.013151 05)(p/R_{\text{air}}^* T_a)$ being the inlet gas density (kg/m^3). $U(x)$ is the control variable defined such that the distribution of secondary-air input $(d\dot{m}_a^*/dx) = U^2(x)$ is positive. From the initial values $R(0) = 1$, $u_l(0) = u_{l0}$, $T_l(0) = T_{l0}$, $u_g(0) = 1$, $Y_F = 0$, $Y_O = 1$, $T_g(0) = 1$, the inlet conditions ($x = 0$) of the state vector are $\mathbf{z}(0) = (1, u_{l0}, T_{l0}, 1, 1, 0, 1, 0)^T$. The target values at the combustor exit ($x = 1$) are chosen as $\mathbf{z}(1) = (0, na, na, na, T_e, 0, na, \dot{m}_1^*/\dot{m}_0^*)^T$, where T_e is the thermodynamically correct exit temperature; na means no target is specified. Q is the constant nondimensional fuel heating value and L_{eff} is the effective heat of vaporization as defined by Sirignano [1]; L^*, A^*, and ν are the chamber length, constant chamber-cross-sectional area, and mass stoichiometric ratio. Models for the internal liquid droplet heating, droplet drag per unit volume D^*, and droplet vaporization rate per unit volume $\dot{M}^*$ are taken from Sirignano [1], sections 2.1.2, 3.1.5, and 3.2, respectively. A perfect gas is assumed. At the low velocities and Mach numbers considered, the pressure variation can be neglected in the equation of state whereas it remains important in the momentum equation.

The first three differential equations above for the liquid phase and the final differential equation are identical in all three models. Droplets are assumed to remain spherical with uniform but time-varying internal liquid temperature. The last terms in the fourth–seventh equations represent the combined effects of gas mixing and chemical reaction. Vaporization produces fuel vapor, increasing the value of the mass fraction Y_F. The mixing rate is determined by a classical eddy-breakup model with the length scale given by using the largest turbulent eddies which are of the order of the chamber dimension and with the turbulent kinetic energy proportional to square of the local gas velocity.

The κ variable in the differential equations contains both the nondimensional characteristic mixing time $\sqrt{A^*}/z_4$ and the nondimensional characteristic chemical time τ_{chem}. The vaporization-mixing model is obtained when τ_{chem} is replaced by zero earlier.

The vaporization model is obtained by suppressing the sixth and seventh differential equations and by replacing the final term in the fourth and fifth equations with $\dot{M}Q$ and $(z_5/z_4)\dot{M}Q$, respectively. More details on the vaporization rate law and drag law are provided in Appendices A and B and in Sirignano et al. [4].

A. Comparison of Models

The models are simplistic but still have five–seven characteristic times, and so they are adequate for this purpose of constructing a framework for optimization of continuous combustors. In our steady-state representation, these time scales are converted to spacial scales. Each model has two (gas and droplet) residence times, a droplet-heating time, a droplet-vaporization time, and a droplet-deceleration time. The vaporization-mixing model adds a gas-mixing time whereas the vaporization-mixing-reaction model adds both a gas-mixing time and a chemical-reaction time. This count does not include the multitime scales that can be associated with the control to be used later, i.e., rate of air addition. And so we do have a rich control challenge.

In the calculations presented in this paper, the total mass flux of air addition equals the mass flow of air flowing through the inlet at $x = 0$. The fuel injection mass flow rate at $x = 0$ is 1.5 times the stoichiometric amount to burn with the inlet air or, equivalently, 0.75 of the stoichiometric amount required to burn the total air flow. In other words, we begin with a fuel-rich situation at $x = 0$ but, with the subsequent air addition, a fuel-lean situation develops.

As can be seen in Fig. 1, the vaporization-mixing model does not burn as much of the fuel as the vaporization model due to the added time accounting for mixing to take place. The vaporization-mixing-reaction model which takes into account the chemical reaction that must take place for the combustion of the fuel and air takes even longer. Note that the chemical reaction has more effect at lower temperatures. We also provide some comparisons between the other states for the vaporization model and vaporization-mixing model. As can be expected, the temperature reaches higher levels in the vaporization model than in the vaporization-mixing model. The gas velocity u_g is also much higher in the vaporization model than in the vaporization and mixing model. This is expected because the higher temperature results in lower density which causes an increase in velocity for the expanding gas. The liquid velocity u_l is higher in the vaporization model than in the vaporization-mixing model. The increased gas velocity resulted in a greater drag force and acceleration of the liquid drops. The liquid temperature T_l is also higher in the vaporization model than in the vaporization-mixing model due to increased heat transfer rates caused by the higher gas temperatures. The Y_F mass fraction in the vaporization and mixing model is very small but has an impact due to the large quantity of energy contained in the fuel.

B. Simulation Analysis and Informal Optimization

We are able to establish some general relationships by simply changing some of the parameters. The base set of parameters is $R_0^* = 80\ \mu\text{m}$, $u_{0l}^* = 15$ m/s, $L^* = .175$ m, $p = 20$ atm, $T_{l0}^* =$ 300 K, and $T_0^* = 900$ K. In the parameter survey, one parameter at a time is varied while the other parameters remain at base values. Briefly, the results follow:
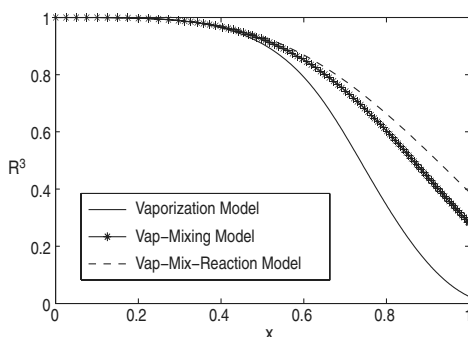
1) As the initial radius decreases, the amount of fuel burned increases monotonically.

2) As the initial liquid velocity decreases, the amount of fuel burned increases monotonically.

3) As the length of the chamber increases, the amount of fuel burned increases monotonically.

4) As the pressure increases, the amount of fuel burned increases monotonically.

5) As the initial liquid temperature increases, the amount of fuel burned increases monotonically.

6) As the initial gas temperature increases, the amount of fuel burned increases monotonically.

Also, as a preliminary step in developing a sense for the optimal air-input rate profile, we compare three different types of air-input rate profiles for the vaporization-mixing model:

1) An exponentially decaying profile $(\mathrm{d}\dot{m}_a/\mathrm{d}x) = (m_1^*/\dot{m}_0^*)(\alpha e^{-\alpha x}/1 - e^{-\alpha})$ where for this computation we choose the parameter $\alpha = 10$. This profile injects almost all of the air near the inlet at the upstream end of the combustion chamber.

2) Another profile compared is a flat profile $(\mathrm{d}\dot{m}_a/\mathrm{d}x) = 1$ which sends a constant amount of air into the chamber over its entire length.

3) A power profile $(\mathrm{d}\dot{m}_a/\mathrm{d}x) = \alpha(m_1^*/\dot{m}_0^*)x^{\alpha-1}$, where we choose the parameter $\alpha = 10$ again but now in a new context, is also considered. This profile injects almost all of the air at the downstream end of the chamber near the flow exit.

We can see from Fig. 2 that the more air that is injected toward the upstream inlet, the more fuel is burned by the exit $x = 1$. The exponentially decaying profile is better than both a flat profile and a power profile. Consequently, we suspect that the optimal control results will yield a distribution weighted toward the upstream inlet for the mass flow rate of air addition.

These first results do not clash in any major way with prior knowledge from more sophisticated computations or empirical data. And so, although our combustion models are substantially simplified, we find them useful for the development of an optimal control approach.

There are two factors that influence the burning of the fuel droplets in opposing ways so as to present an interesting control problem. As we inject more of air into the chamber of given cross-sectional area near the upstream inlet, the gas velocity is increased. Consequently, the droplet drag increases and the droplet will accelerate more because of the air addition and spend less time in the combustion chamber, having less time to completely burn. However, the injection of air in the upstream portion of the chamber would also increase the droplet Reynolds number and thus vaporize and burn the droplet more quickly. And so some challenge exists to bring the proper balance here.

III. Optimal Control Framework

We first formulate the problem as an optimal control problem in continuous time (really space in this problem) over the fixed interval

Fig. 1 Comparison of nondimensional droplet volume amongst the three models.
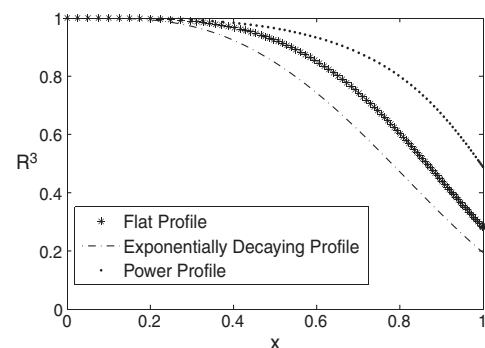
Fig. 2 Comparison amongst different air-addition profiles for the vaporization-mixing model.

$0 \leq x \leq 1$, with the system dynamics given by (1) and compactly expressed here as

$$\dot{\mathbf{z}}(x) = \mathbf{f}(\mathbf{z}(x), U(x)); \qquad \mathbf{z}(0) = \mathbf{z}_0 \qquad (2)$$

and with the initial conditions $\mathbf{z_0} = (1, \quad u_{l_0}, \quad T_{l_0}, \quad 1, \quad 1, \quad 0,$ $1, 0)^T$ defined in Sec. II. We can then formulate the continuous-time optimal control problem as

$$\min_{U,\mathbf{z}} J^C = \Phi(\mathbf{z}(x=1)) + \int_0^1 l(\mathbf{z}(x), U(x))\mathrm{d}x$$
$$\dot{\mathbf{z}}(x) = \mathbf{f}(\mathbf{z}(x), U(x)) \qquad \mathbf{z}(0) = \mathbf{z}_0 \qquad (3)$$

where J^C is the cost function that we wish to minimize and Φ, $l(\mathbf{z}, U)$ are selected as discussed later to achieve the design objectives. A general discussion of optimal control problems can be found in Luenberger [5]. We remark again that we use the square of the control U to express $(\mathrm{d}\dot{m}_a/\mathrm{d}x) = U^2$ so that we can avoid imposing additional constraints on the control in (3) to keep $\mathrm{d}\dot{m}_a/\mathrm{d}x$ positive when we optimize over U. For computational purposes, the continuous-time optimal control problem is first discretized. More specifically, using a Runge-Kutta formulation, the continuous space of x from 0 to 1 is discretized into $N + 1$ points from $n = 0$ to $n = N$ and we obtain the following discrete-time optimal control problem:

$$\min_{U,\mathbf{z}} J^D = \Phi(\mathbf{z}(N)) + \sum_{n=0}^{N-1} L(\mathbf{z}(n), U(n), n) \qquad (4)$$

subject to

$$\mathbf{z}(n+1) = \mathbf{F}(\mathbf{z}(n), U(n)); \qquad \mathbf{z}(0) = \mathbf{z}_0 \qquad (5)$$

where the functions F and L result from f and l, respectively, through the discretization of the continuous-time optimal control problem.

The cost function J^D has a terminal penalty term $\Phi(\mathbf{z}(N))$ which enforces the desired end states, as well as the running cost penalty

$$\sum_{n=0}^{N-1} L(\mathbf{z}(n), U(n), n)$$

which dictates what values we wish the states to take over the entire space of the combustion chamber. By minimizing the cost function, we come closer to our targets for the state vector $\mathbf{z}$. We choose the cost function J^D (and clearly J^C) to be quadratic, namely, we define Φ and L as follows:

$$L(\mathbf{z}(n), U(n), n) = \frac{1}{2}[\mathbf{z}(n) - \mathbf{z}_t(n)]^T \mathbf{Q}(n)[\mathbf{z}(n) - \mathbf{z}_t(n)]$$
$$+ \frac{1}{2}[U(n) - U_t(n)]^T R(n)[U(n) - U_t(n)] \qquad (6)$$

$$\Phi(z) = \frac{1}{2}[\mathbf{z} - \mathbf{z}_t(N)]^T \mathbf{Q}(N)[\mathbf{z} - \mathbf{z}_t(N)] \qquad (7)$$

where $\mathbf{z}_t$ is the state target, and we define the penalty matrix $\mathbf{Q}(N)$ with the penalties on the final states as

$$\mathbf{Q}(N) = (10^4, 0, 0, 0, 10^4, 10^4, 0, 10^4)^T \qquad (8)$$

In addition, we are only interested in reaching the target state values: we want all of the fuel to be burned at $n = N$, the gas temperature to leave the chamber at the correct thermodynamic exit temperature T_e, and the proper amount of air $\dot{m}_1^*/\dot{m}_0^*$ injected over the length of the chamber. Therefore, we set $\mathbf{Q}(n)$ to 0 for $0 \leq n \leq N - 1$. Note that in this problem $U(n)$ is a scalar but in principle it could be a vector containing multiple controls. $R(n)$ are penalties used to keep the controls $U(n)$ near specified target values $U_t(n)$ and, in particular, when $U_t(n) = 0$ as in our case to guard against large control values; if no such objective is necessary, $R(n)$ can be taken small but for technical reasons cannot be set equal to zero. Here we take $R(n) = 4$ for all n.

The optimal control is found iteratively using the SLQ algorithm developed by Sideris and Bobrow [2] to solve nonlinear discrete-time optimal control problems. More specifically, let the current control sequence be $\mathbf{U}_m = [U(0) \cdots U(n) \cdots U(N-1)]^T$ at iteration m, with the corresponding states [solved from Eq. (5)] being $\mathbf{Z}_m = [\mathbf{z}^T(0) \cdots \mathbf{z}^T(n) \cdots \mathbf{z}^T(N)]^T$. The state dynamics are then linearized about $\mathbf{U}_m$ and $\mathbf{Z}_m$ to give $\bar{\mathbf{z}}(n+1) = \mathbf{F}_z(\mathbf{z}(n), U(n))\bar{\mathbf{z}}(n) + \mathbf{F}_U(\mathbf{z}(n), U(n))\bar{U}(n)$ where $\mathbf{F}_z = (\partial \mathbf{F}/\partial z)$ and $\mathbf{F}_U = (\partial \mathbf{F}/\partial U)$. Note that we use a bar to denote deviations from their nominal values of corresponding variables in the linearized version of the problem. Let also $\bar{J}^D$ denote the cost index J^D as a function of $\bar{U}(n)$ and $\bar{\mathbf{z}}(n)$, after substituting $U(n) + \bar{U}(n)$ and $\mathbf{z}(n) + \bar{\mathbf{z}}(n)$ for $U(n)$ and $\mathbf{z}(n)$, respectively. Minimizing $\bar{J}^D$ over $\bar{U}(n)$ and $\bar{\mathbf{z}}(n)$, subject to the linearized dynamics and with initial state $\bar{\mathbf{z}}(0) = 0$, yields an optimal solution $\bar{\mathbf{U}}_m = [\bar{U}(0) \cdots \bar{U}(n) \cdots \bar{U}^T(N-1)]^T$. Then we perform a step from $\mathbf{U}_m$ in the direction defined by $\bar{\mathbf{U}}_m$ to compute the next control $\mathbf{U}_{m+1}$ as follows:

$$\mathbf{U}_{m+1} = \mathbf{U}_m + \alpha_m \bar{\mathbf{U}}_m \qquad (9)$$

where we choose α_m by solving the 1-D search problem

$$\min_{0 < \alpha_m \leq 1} J[\mathbf{U}_m + \alpha_m \bar{\mathbf{U}}_m] \qquad (10)$$

Essentially, we step as far as $\mathbf{U}_m + \bar{\mathbf{U}}_m$ in the direction determined by $\bar{\mathbf{U}}_m$ as long as the cost is not increasing. The SLQ algorithm guarantees that $\bar{\mathbf{U}}_m$ is a descent direction and that $\mathbf{U}_m$ converges to a solution such that the first-order optimality conditions (11–14) as described below are satisfied [2]:

$$\mathbf{z}(n+1) = \mathbf{F}(\mathbf{z}(n), U(n)); \qquad \mathbf{z}(0) = \mathbf{z}_0 \qquad (11)$$

$$\boldsymbol{\lambda}^T(n) = \boldsymbol{\lambda}^T(n+1)\mathbf{F}_z(\mathbf{z}(n), U(n)) + L_z(\mathbf{z}(n), U(n)) \qquad (12)$$

$$\boldsymbol{\lambda}(N) = \Phi_z(\mathbf{z}(n)) \qquad (13)$$

$$0 = H_u(\boldsymbol{\lambda}(n+1), \mathbf{z}(n), U(n)) \qquad (14)$$

where $\boldsymbol{\lambda}(n)$ is the adjoint trajectory and H is the Hamiltonian defined by

$$H(\boldsymbol{\lambda}, \mathbf{z}, U) = \boldsymbol{\lambda}^T \mathbf{F}(\mathbf{z}, U) + L(\mathbf{z}, u) \qquad (15)$$

More details on the optimization analysis can be found in Appendix C of Sirignano et al. [4].

IV.   Results and Discussion

A.   Results for Vaporization-Controlling Model

As mentioned earlier, there are two factors that influence the burning of the fuel droplets. Upstream injection of the air causes more acceleration and a lower residence time in the chamber for the droplet. However, the upstream injection of air would also increase the droplet Reynolds number and thus cause the droplet to vaporize more quickly. The vaporization model has the least number of characteristic times because mixing time and chemical time are implicitly equal to zero. And so, the optimization here is not as subtle as for the other models. We choose to optimize under parameters such that with a flat profile there is less than 10% of unburned fuel at the chamber exit. Then, optimizing under the parameters $L^* = .4$ m, $R_0^* = 70$ μm, $u_{l0}^* = 30$ m/s, $u_{g0}^* = 40$ m/s, $T_0^* = 900$ K, $T_{l0}^* = 300$ K, and $p = 10$ atm, we find the optimal function for $\mathrm{d}\dot{m}_a/\mathrm{d}x$ to be such that the air is injected mostly near the upstream inlet, conforming to an exponentially decaying profile. The latter factor, the increased burning of the droplet due to the higher Reynolds number, is then the dominant one of the two. Then, as the discretization grid becomes finer, the optimal control for $\mathrm{d}\dot{m}_a/\mathrm{d}x$ tends to a delta function at $x = 0$.
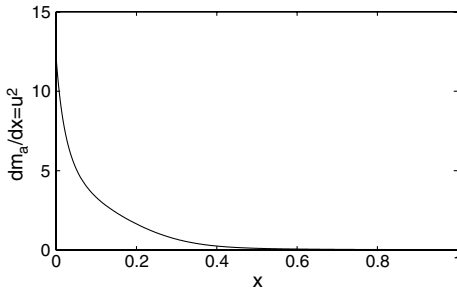
Fig. 3   Control for vaporization model with constraint on maximum rate of air addition.

Because this solution is physically unacceptable, we impose a maximum on the control by using a sigmoid function; with this constraint, the resulting optimal air profile exponentially decays more gradually and is depicted in Fig. 3. The corresponding states for the optimal profile are shown in Fig. 4. We can observe that the droplet radius R has practically converged to 0 at the end of the combustor as required.

B.   Results for Vaporization and Mixing Model

For the vaporization-mixing model, we consider here an initial droplet radius $R_0^* = 60 \ \mu$m, $L^* = 0.4$ m, $u_{l0}^* = 30$ m/s, $u_{g0}^* = 40$ m/s, $T_0^* = 900$ K, $T_{l0}^* = 300$ K, and $p = 10$ atm. The results for the second model indicate a slower burning than found for the vaporization model even though the preceding model calculation had a larger initial droplet size. So that, as expected, the mixing process takes more time. Results are shown in Figs. 5 and 6. It is still optimal to inject the air toward the beginning of the chamber. It can be observed that droplet volume R^3 and the fuel vapor mass fraction Y_F achieve very low values at the end of the combustor. These values can be further optimized toward zero if desired by selecting higher penalty terms for the corresponding states in (8).

C.   Results for Vaporization-Mixing-Reaction Model

For the vaporization-mixing-reaction model, we use the same parameters as with the vaporization-mixing model. The general results for this model are shown in Figs. 7 and 8. It is again optimal to
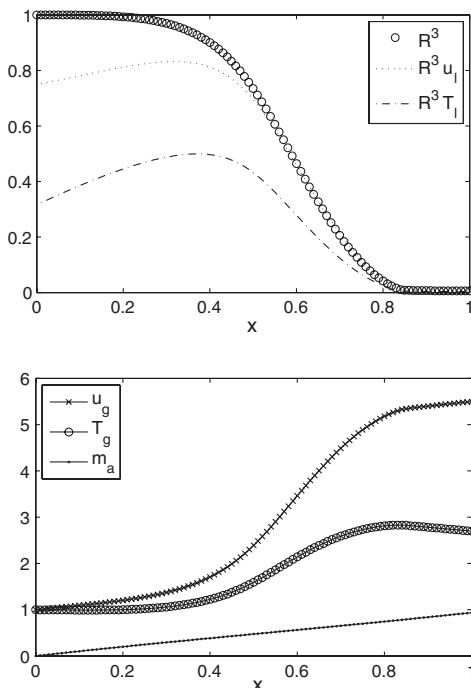
Fig. 4   States with constraint on maximum rate of air addition: a) liquid-phase variables, and b) gas-phase variables.
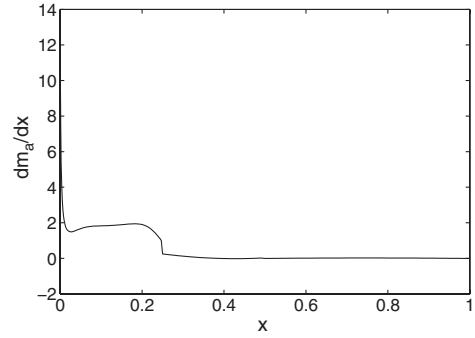
Fig. 5   Optimal control for vaporization-mixing model: rate of air addition.
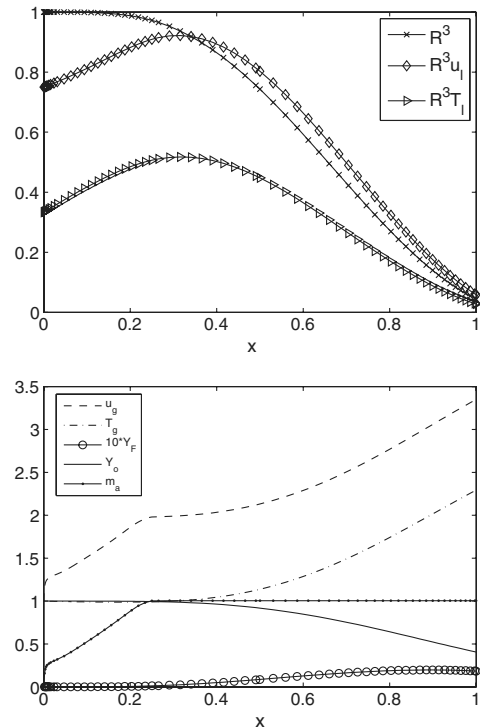
Fig. 6   States for vaporization-mixing model: a) liquid-phase variables, and b) gas-phase variables.

inject most of the air at the beginning of the combustion chamber. However, a secondary pulse of air injection is provided downstream. The air addition follows just downstream of the beginning of the temperature increase. Sufficient vaporization and reaction has occurred for the chemical reaction to begin. Presumably, if more air had been injected upstream, the gas temperature would have been forced downward, delaying ignition and slowing droplet heating and vaporization, and so the optimization procedure found a more
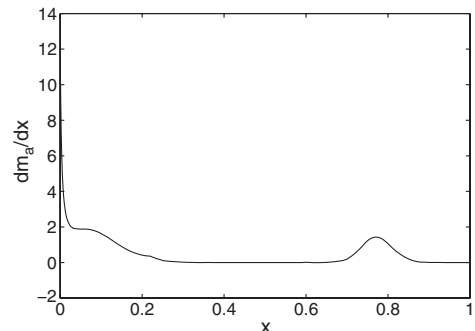
Fig. 7   Optimal control for vaporization-mixing-reaction model.
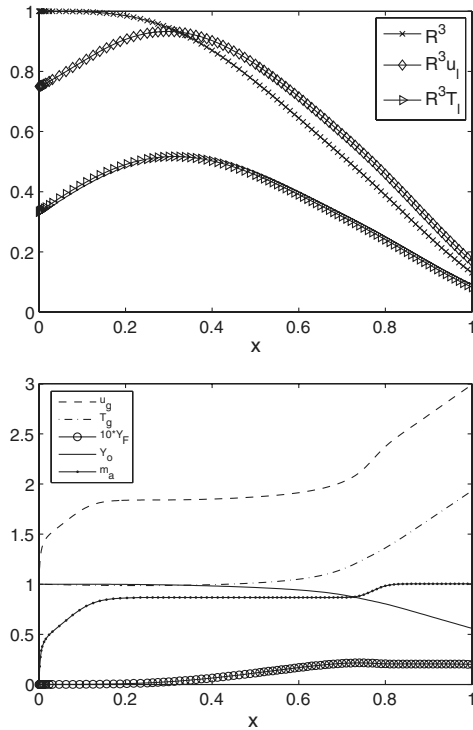
Fig. 8 States for vaporization-mixing-reaction model: a) liquid-phase variables, and b) gas-phase variables.

interesting distribution for the air addition. Still, the droplet volume R^3 and the fuel vapor mass fraction Y_F maintain higher values at the end of the combustor than the values found in the preceding models. Clearly, the addition of the chemical time slows the burning process. These final exit values can be further optimized toward zero by selecting higher penalty terms for the corresponding states in (8). If the initial gas temperature were lowered, the chemical time could increase significantly because of the exponential dependence.

V. Conclusions

Three combustion models have been proposed. In order of increasing complexity and increasing number of characteristic times, they are a vaporization-controlling model, a vaporization-mixing model, and a vaporization-mixing-reaction model. The vaporization-mixing model takes longer than the vaporization-controlling model for the fuel to be burned due to the added time needed for the fuel and air to mix. The burning with the vaporization-mixing-reaction model is still slower than with the vaporization-mixing model, implying that the chemical reaction does take an additional amount of time to occur. At lower initial temperature the time for the chemical reaction to take place will be higher.

The behaviors of all of the models are monotonic in certain parameters including initial radius, initial liquid velocity, length of the chamber, pressure, and initial liquid temperature. As each of these parameters increases, the amount of fuel burned decreases, decreases, increases, increases, and increases, respectively.

Informal attempts at optimization using monotonic air-addition profiles are shown to be limited in capability. With this informal process, we show that the burning of the fuel appears to be not too highly sensitive to our choice of a specific air injection monotonic profile, with modest changes to the amount of liquid fuel vaporized depending upon which profile we choose. Injecting more of the air upstream produces an improvement of a few percent more of the original amount of fuel vaporized than when choosing a flat profile, as shown in Fig. 2. Still more improvement is found in comparison with the power profile that injects most of the air toward the downstream end of the chamber. Note that the ranking of the air-input profiles are somewhat invariant under different lengths of the

chamber; it is always advantageous to inject the air at the upstream end.

We find much more interesting and improved results with the formal optimization process. Using the SLQ algorithm, we were able to find the optimal air-input profile along the chamber. The optimal choice is generally to inject most of the air upstream. However, Figs. 5 and 7 show that the optimal rate of air addition can have local peaks at more than the inlet because of the added characteristic times.

There are two factors which influence whether it is optimal to inject the air at the upstream location: first, the Reynolds number will be higher and the fuel will be burned faster, but, second, the air will accelerate the fuel droplets causing them to spend less time in the chamber and consequently not have as much time to completely burn. The optimal control result suggests that the former is the stronger factor.

There are some differences between the optimal air profile for the vaporization model and the vaporization-mixing model. Although both inject most of the air at the upstream end of the chamber, the latter does so much more gradually whereas the former (without any constraints on its maximum) seeks to inject it all initially at $x = 0$. This is consistent with our understanding of the models; the vaporization-mixing model must allow for more time for the fuel and air to mix. Consequently, more air is injected later when the mixing has been completed. The vaporization model has no need to wait for the completion of the mixing because it has approximated it as an instantaneous process. The optimization process for the vaporization-mixing-reaction model clearly creates a second pulse of air addition downstream, which occurs once vaporization and mixing processes are sufficiently advanced and the ignition has occurred.

The framework developed here with the SLQ algorihm offers promise for application to other choices of control variables for optimal control of continuous combustors and to other more detailed combustion models with higher dimensions.

The authors are unaware of available experimental or computational data in which variations of secondary-air configurations have been studied. And so, at this time, comparisons are not possible. The results of this paper could motivate future studies of that type.

Appendix A: Determination of Vaporization Rate

The vaporization rate of an individual droplet is taken as a positive number and can be written as

$$\dot{m}_d^* = \frac{|\dot{M}^*|}{n^*} \qquad (A1)$$

where n^* is the number of droplets per unit volume. From Sirignano [1], for Schmidt number equal to one, the individual-droplet vaporization rate for a droplet moving relative to the surrounding gas can be represented as

$$\dot{m}_d^* = 4\pi\rho^*\tilde{D}^*R^*\log(1+B)\left[1 + \frac{Re}{2}e^{-Re}\right.$$

$$\left. + \frac{0.6(2Re)^{0.5}(1-e^{-Re})}{F(B)}\right] \qquad (A2)$$

where $\tilde{D}^*$ is the mass diffusivity. The Reynolds number Re, transfer number B, and function $F(B)$ are given by

$$Re = \rho|u_g - u_l|R\frac{\rho_0^*|u_0^* - u_{l0}^*|R_0^*}{\mu_0^*} \qquad (A3)$$

$$B = \frac{Y_{Fs}}{1 - Y_{Fs}} \qquad (A4)$$

$$F(B) = [1+B]^{0.7}\frac{\log(1+B)}{B} \qquad (A5)$$

where μ_0^* is the dynamic viscosity which is assumed to be constant and Y_{Fs} is the mass fraction of fuel vapor in the gas at the droplet surface.

The mass fraction of fuel vapor at the surface is a strong function of liquid temperature, fuel properties, and pressure. In particular

$$Y_{Fs} = (1/p^*)e^{\text{La}^*/(\bar{R}^* T_b^*)} e^{-\text{La}/T_l} \tag{A6}$$

where T_b^* is the boiling point at 1 atm of pressure $\text{La} = \text{La}^*/(\bar{R}^* T_0^*)$, p^* here must be measured in atmospheres, and $\bar{R}^*$ is the gas constant for the liquid species (i.e., the universal gas constant divided by molecular weight).

It can also be shown [1] that

$$L_{\text{eff}} = \frac{L_{\text{eff}}^*}{c_p^* T_0^*} \frac{T - T_l}{B} \tag{A7}$$

To avoid a singularity condition in the differential equations as R approaches zero, we introduce a sigmoid σ_1 to halt the calculations if R is less than a small number ϵ_1. Similarly, if there is no oxygen left to burn, we do not wish the model to continue burning the droplet. This second sigmoid σ_2 stops the calculations if the air mass fraction Y_O drops below a small number ϵ_2. More specifically, we define

$$\sigma_1 = \frac{1}{1 + e^{-\lambda_1(z_1 - \epsilon_1)}} \tag{A8}$$

$$\sigma_2 = \frac{1}{1 + e^{-\lambda_2(Y_O - \epsilon_2)}} \tag{A9}$$

Then, if we define $h = (1 + .5Re)e^{-Re} + .42\frac{Re^{1/2}}{F}(1 - e^{-Re})$, the vaporization rate becomes

$$\dot{M} = 4\pi c_1 \sigma_1 \sigma_2 \frac{z_1^{4/3}}{z_2} \ln(1 + B)h \tag{A10}$$

Equation (A2) has the mass rate of vaporization becoming proportional to Re for low Re and becoming proportional to $Re^{1/2}$ for large Re.

Appendix B: Determination of Drag Force

The drag per unit volume on droplets is given by

$$D^* = n^* C_D \frac{1}{2} \rho^* (u^* - u_l^*) |u^* - u_l^*| \pi R^{*2} \tag{B1}$$

For a vaporizing droplet, we can state

$$C_D = \frac{12}{Re(1 + B)} \tag{B2}$$

Now the nondimensional drag may be written as

$$D = \frac{D^* L^*}{\rho_0^* u_0^{*2}} = \frac{6\pi c_1}{(1 + B)} \frac{(u - u_l)R}{u_l} \tag{B3}$$

where the constant c_1 is defined as

$$c_1 = \frac{3\rho_0^*}{4\pi \rho_l^*} \frac{\mu_0^* \dot{m}_f^*}{\dot{m}_0^{*2}} \frac{L^* A^*}{R_0^{*2}} \tag{B4}$$

Note that the chamber length L^* appears only through the constant c_1.

References

[1] Sirignano, W. A., *Fluid Dynamics and Transport of Droplets and Spray*, 2nd ed., Cambridge Univ. Press, New York, 2010.

[2] Sideris, A., and Bobrow, J. E., "An Efficient Sequential Linear Quadratic Algorithm for Solving Nonlinear Optimal Control Problems," *IEEE Transactions on Automatic Control*, Vol. 50, No. 12, Dec. 2005, pp. 2043–2047.
doi:10.1109/TAC.2005.860248.

[3] Ge, H. W., Shi, Y., Reitz, R. D., Wickman, D. D., and Willems, W., "Optimization of a HSDI Diesel Engine for Passenger Cars Using a Multi-Objective Genetic Algorithm and Multi-Dimensional Modeling," SAE World Congress & Exhibition Paper 2009-01-0715, April 2009.

[4] Sirignano, J. A., Rodriquez, L., Sideris, A., and Sirignano, W. A., "One-Dimensional Spray Combustion Optimization with a Sequential Linear Quadratic Algorithm," Combustion Institute, Paper 32I3, Pittsburgh, PA, May 2009.

[5] Luenberger, D. G., *Introduction to Dynamic Systems: Theory, Models, and Applications*, Wiley, New York, 1979.

A. Gupta
Associate Editor